Biophysical Journal
Article

Biophysical Society

Antibody binding modulates the dynamics of the membrane-bound prion protein

Ioana M. Ilie,[1] Marco Bacci,[1] Andreas Vitalis,[1] and Amedeo Caflisch[1,*]
[1]Department of Biochemistry, University of Zürich, Zürich, Switzerland

ABSTRACT Misfolding of the cellular prion protein (PrP^C) is associated with lethal neurodegeneration. PrP^C consists of a flexible tail (residues 23–123) and a globular domain (residues 124–231) whose C-terminal end is anchored to the cell membrane. The neurotoxic antibody POM1 and the innocuous antibody POM6 recognize the globular domain. Experimental evidence indicates that POM1 binding to PrP^C emulates the influence on PrP^C of the misfolded prion protein (PrP^{Sc}) while the binding of POM6 has the opposite biological response. Little is known about the potential interactions between flexible tail, globular domain, and the membrane. Here, we used atomistic simulations to investigate how these interactions are modulated by the binding of the Fab fragments of POM1 and POM6 to PrP^C and by interstitial sequence truncations to the flexible tail. The simulations show that the binding of the antibodies restricts the range of orientations of the globular domain with respect to the membrane and decreases the distance between tail and membrane. Five of the six sequence truncations influence only marginally this distance and the contact patterns between tail and globular domain. The only exception is a truncation coupled to a charge inversion mutation of four N-terminal residues, which increases the distance of the flexible tail from the membrane. The interactions of the flexible tail and globular domain are modulated differently by the two antibodies.

SIGNIFICANCE Antibody binding modulates the toxicity of the cellular prion protein. Using computer simulations, we show that the interactions of the protein's flexible tail and its folded, globular domain are modulated differently by two antibodies with contrasting biological response. We find that the antibodies restrict the orientations of the globular domain relative to the membrane and decrease the distance of the flexible tail to its surface. We show that interstitial truncations in the flexible tail have comparable effects, except for a mutant introducing a charge inversion. Thus, this study provides an atomistic description of the mediating role of the flexible tail in the presence of both a toxic and an innocuous antibody and for various, experimentally studied tail truncations.

INTRODUCTION

Prion diseases or transmissible spongiform encephalopathies (TSEs) are neurodegenerative disorders, known as Creutzfeldt-Jakob disease in humans, spongiform encephalopathy (mad cow disease) in bovines, scrapie in sheep, or chronic wasting disease in deer. TSEs are linked to the misfolding and aggregation of the cellular prion protein (PrP^C) into the insoluble and toxic isoform PrP^{Sc} (scrapie) (1), which then propagates itself by imposing its conformation onto PrP^C. PrP^C is a cell-surface glycoprotein (2), which was shown to facilitate myelin homeostasis by flexible tail-mediated agonism of the G-protein-coupled receptor ADGRG6 (also called GPR126) (3).

Structurally, the nonpathogenic PrP^C consists of a long flexible tail (residues 23–123) and a globular domain (residues 124–231) (Fig. 1). The first 22 residues are cleaved during trafficking and the segment 232–253 is replaced by a glycosyl-phosphatidylinositol anchor (GPI anchor), which enables membrane attachment (4). The flexible tail includes an N-terminal, positively charged five-residue segment (charge cluster 1, abbreviated CC1, residues ^{23}KKRPK^{27}), an octarepeat region (residues 50–90), and a C-terminal, positively charged segment (CC2, residues 95–110). The globular domain is composed of an anti-parallel β-sheet formed between residues 128–131 (β_1) and 160–162 (β_2), and three α-helices comprising residues 143–155, 171–192, and 199–226 (α_1, α_2, and α_3), with the latter two stabilized by a disulfide bond. The pathogenic isoform PrP^{Sc} is rich in β-sheets, is insoluble, and has a high propensity to aggregate into amyloid-like fibrils (5).

Submitted January 5, 2022, and accepted for publication June 1, 2022.
*Correspondence: caflisch@bioc.uzh.ch
Editor: Alan Grossfield.
https://doi.org/10.1016/j.bpj.2022.06.007

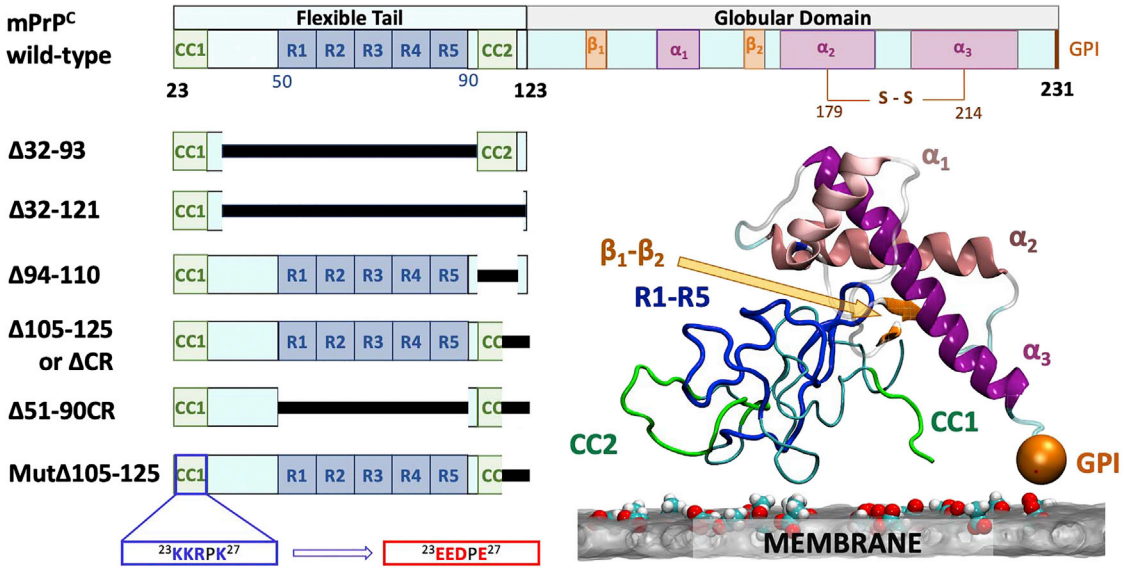

FIGURE 1 Unliganded PrP^C simulation systems. Schematic illustration of the sequence of mouse PrP^C ($mPrP^C$) and the mutants with interstitial deletions in the flexible tail. For the mutants, only the flexible tail is shown. The flexible tail (residues 23–123) includes two charged clusters (CC1 and CC2) and five octapeptide repeats (R1 to R5, residues 50–90) while the globular domain (residues 124–231) includes two β-strands and three α-helices. In all simulations, the globular domain of PrP^C was anchored at the membrane surface to mimic the C-terminal glycosyl-phosphatidylinositol (GPI) and restrained to remain folded. Only wild-type PrP^C was used for the simulations of the complexes with POM1 and POM6. In the snapshot on the right, the elements in the schematic representation are highlighted by matching colors on the wild-type $mPrP^C$ structure. To see this figure in color, go online.

A proposed therapeutic approach to avoid the pathogenic transformation into PrP^{Sc} is to develop monoclonal antibodies that bind to PrP^C and stabilize its native structure (8). Some of these antibodies have been shown to reduce the amount of scrapie prion both *in vitro* and *in vivo* (8). The POM family of monoclonal antibodies has been developed to recognize a variety of epitopes along the sequence of PrP^C (9). Antibodies recognizing epitopes in the octarepeat region, e.g., POM2, POM11, and POM12, were shown to be innocuous (10). Similarly, POM6, with a sequence-discontinuous epitope in the globular domain, is also innocuous (10). In contrast, while the POM1 antibody has an epitope in the globular domain similar to that of POM6 (β_1-α_1 loop, N-terminal turn of helix α_1, and part of helix α_3), it is generally neurotoxic. Interestingly, mutants devoid of the octarepeat region (Δ32–93) are resistant to POM1-induced toxicity whereas CC2-truncated proteins (Δ94–110) record POM1-induced neurodegeneration (10). The Aguzzi group has proposed that neurotoxicity is a consequence of the docking of POM1 to PrP^C, which may emulate the binding of PrP^{Sc}, and is mediated by the flexible tail (10,11).

Extensive experimental efforts have been dedicated to investigating the effects of various truncations in the flexible tail and their roles in modulating prion-induced neurotoxicity and neuroprotection (12). Using scrapie-infected mouse neuroblastoma cells, it was demonstrated that the deletion of the octarepeat region did not alter PrP^{Sc} synthesis, yet it required longer incubation times than wild-type PrP^C (13,14). Furthermore, the deletion mutant restored susceptibility of PrP^C knockout mice to scrapie, allowing prion propagation and accumulation (14). Transgenic mice expressing PrP^C devoid of the 32–93 sequence showed no signs of neurotoxicity, whereas those expressing longer truncations, i.e., 32–121 or 32–134, were displaying severe ataxia and neuronal death (15). The expression of 105–125 truncated PrP^C (Δ105–125) in transgenic mice resulted in clear signs of neurodegeneration, which ultimately led to death (16). On the other hand, transgenic mice expressing PrP^C devoid of the CC2 domain (residues 94–110) did not develop chronic demyelinating polyneuropathy (CDP) (17), whereas mice expressing PrP^C lacking the 94–134 domain did develop CDP (18). Additionally, the effects of the latter and of Δ105–125 could be reversed by expression of wild-type PrP^C (16,18). It should be kept in mind throughout that animal models of the disease have advanced tremendously but do not always offer simple, causal interpretations (19).

Recent studies correlate the generation of spontaneous ionic currents when expressing PrP^C truncations in transfected cell lines with toxicity (12,20,21). As an example, results from drug-based cellular assays and patch-clamp assays indicate that the expression of the Δ105–125 deletion in cells incurs large cationic channel activities and a decrease in cell viability (20,22). The CC1 domain (residues 23–27) seems to play an essential role in the channel activity of Δ105–125 (20). In particular, mutations of the positively charged residues in the CC1 sequence (^{23}KKRPK^{27}) to negatively charged (^{23}EEDPE^{27}) ones did not show any ionic currents (23). Cell-based experiments provide information on prion-induced toxicity, but they encounter difficulties in exploring the structural details and dynamics at the atomistic

level. Computer simulations are a complementary tool to explore, capture, and explain phenomena exceeding experimental spatiotemporal resolutions (24–26). Examples of atomistic simulations include studies of the conformations of the monomeric state of PrP^C in solution (27), the dimerization process of amyloidogenic peptides (28), and amyloid fibril elongation (29–31). To date, simulation studies of the prion protein have focused mainly on the globular domain (32,33), with only fragments of the flexible tails attached (34). Furthermore, mutations of residues involved in the stability of the globular domain (27,35,36) and interactions of the globular domain with antibodies (37) are challenging but appealing targets for simulation studies.

Here, we analyze the effects of different interstitial truncations in the flexible tail of PrP^C (Fig. 1), and the binding of the POM1 and POM6 antibodies by implicit solvent simulations with a simplified model of the membrane surface (see materials and methods). The flexible tail poses a huge challenge due to its length, intrinsic disorder, and comparatively hydrophobic sequence composition (the net charge per residue is only 0.1, and there are only the two aforementioned clusters containing a total of 11 charged residues) requiring the use of implicit solvent and simplified membrane surface.

MATERIALS AND METHODS

System preparation

The starting configurations for the systems below were derived from the solution nuclear magnetic resonance structure of the globular domain of mouse PrP^C (PDB: 1XYX (38)), the X-ray diffraction structure of POM1 complexed with the mouse prion protein (PDB: 4H88 (10)), and the X-ray diffraction structure of POM6 in complex with the mouse prion protein (PDB: 6AQ7 (7)). Simulations of POM1- and POM6-bound PrP^C were performed only for the full-length sequence of PrP^C (mouse wild-type residues 23–231). Simulations of unliganded PrP^C were carried out with the wild-type and the following six interstitial truncations in the flexible tail (Fig. 1):

- the Δ32–93 mutant, which requires longer incubation times than wild-type and does not alter PrP^{Sc} synthesis (14);
- the mutant devoid of the Δ32–121 sequence, which causes severe ataxia and neuronal death (15);
- the Δ94–110 truncation, which gave rise to conflicting results: it was reported that there is no toxic influence on mice (17), yet it produces a large ionic channel activity (20);
- the mutant devoid of the central region (Δ105–125), which induces cell death (16);
- the mutant devoid of the octapeptide repeats and central region (Δ51–90CR), which showed increased levels of cell death (20,22);
- the CC1 mutated prion protein (MutΔ105–125), which abolishes the ion current activity of Δ105–125 (20).

For the unliganded systems, missing residues, in particular those in the flexible tail, were constructed according to Engh-Huber covalent geometries (39). Their dihedral angles were randomized using a CAMPARI-specific scheme obeying excluded volume interactions (http://campari.sourceforge.net). This was done independently for every single copy. We were not interested in sampling the ordered parts (see below), so this procedure ensures independent starting configurations for the most relevant entity, namely the flexible tail.

To assemble the complexes with POM1 and POM6, we relied on preliminary simulations. From models constructed by superposing the crystallographic structures with wild-type simulation structures, we identified suitably compatible snapshots that could accommodate both tail and antibody. The end points of those simulations, which were propagated using identical protocols as described below, were extracted, and the flexible tail and the ionic bath were deleted. This yielded structures of stable antibody/PrP^C complexes in the presence of the membrane and with all other missing atoms reconstructed. From a handful of these, we started separate runs in which the missing tail and the ions were constructed randomly but in accordance with volume exclusion. This gave rise to ca. 80 independent tail and bath conformations. These tail conformations are not at all at equilibrium with respect to the target conditions, which favor collapse. Thus, to prevent this artifact from introducing bias, these systems were propagated in the presence of exhaustive half-sided restraints between the C_α-atoms of residues 1–100 in the flexible tail and the C_α-atoms of the antibody (strength 0.1 kcal/mol/Å^2, threshold distance 8.0 Å, 100×431 and 100×430 restraints for POM1/POM6, respectively). This was done to prevent extended tail conformations from getting stuck on the surface of the antibody. The systems were equilibrated in this manner for 5 million steps at temperatures ranging from 350 K to 440 K using a protocol similar to that described in the section "production simulations," yet devoid of the Monte Carlo moves. By visual inspection, this was sufficient to achieve proper, independent starting points of different random tail conformations. The goal of this overall protocol was to mimic the process of the antibody binding to PrP^C while the latter is at equilibrium with its surroundings. It proved necessary based on the analysis of the aforementioned preliminary simulations.

Additionally, in the preliminary runs, both antibody-PrP^C interfaces proved to be at least partially unstable without optimization. For POM1, we identified the buried carboxyl groups of D143 and D146 as culprits. To address this issue, the POM1/PrP^C system was generated by neutralizing both aspartates. Both explicit solvent simulations (I.M.I. and A.C., unpublished data) and the preliminary runs here revealed the POM6/PrP^C interface to be more volatile in general. To avoid the dissociation of the POM6/PrP^C complex at high temperatures, the solvation free energy of the glutamates and the lysine at the interface was adjusted to −50 kcal/mol, H34 in the heavy chain of POM6 was protonated, and a minimalistic set of harmonic restraints was applied between residues at the interface. Specifically, harmonic potentials restrained individual distances between nearby atoms of K181-E184, V180-HC:F32, E177-HC:H34, E123-HC:Q99 E129-LC:Y34 Y126-LC:Y36, and T176-LC:W96 to an upper limit of ca. 5.0 Å, where HC and LC refer to heavy and light chain, respectively. All starting structures of the complex simulations are available at https://gitlab.com/CaflischLab/PrionImplicit.

The simulations were performed using the ABSINTH implicit solvent model (40) with published parameters except for the partial charges, which were taken from the CHARMM36 force field (41) as in recent work (42). In explicit solvent simulations, a high amount of computational cost arises from the interactions within the solvent bath in a bulk solution. In the ABSINTH model, solvation effects are decomposed into a direct mean-field interaction (DMFI) and a screening term for polar interactions. The use of an implicit model is of particular benefit here, as the studied systems consist of up to 640 residues (100 of which being largely unstructured) and require exceptionally large simulations boxes (here 25 nm per edge). The ABSINTH model has been employed in a large variety of simulation studies ranging from the conformational landscape of amyloid peptides in the monomeric state (43) to the self-assembly of diphenylalanine peptides into nanotubes (44).

Membrane model and ions

To characterize the events at the membrane surface at a reasonable computational cost, we introduce here a stylized membrane model intended to capture the essential characteristics of the surface of a neuronal membrane.

This mimic uses the simplest anionic function, carboxylates in acetate molecules, to represent different sources of negative membrane surface charge. Following this logic, we represent the excess in charge simply as 100 acetate anions whose centers of mass are constrained to move in the (x,y)-plane at the bottom of the simulation box (see Fig. 1 *snapshot*). To determine the required anion concentration, we assumed an area per headgroup of approximately 0.6 nm^2 (45), which translates into an assumed fraction of negatively charged lipids (predominantly phosphatidylserine and different phosphatidylinositol phosphates) of approximately 0.1 in our model. Due to the asymmetry of the environment and missing parameters, membrane insertion is a difficult process to simulate accurately in continuum models. Because here insertion would have to be coupled to the conformational equilibrium of the tail, we limited the scope of the present study by restricting ourselves to modeling a nearby but impenetrable membrane. In practice, the impenetrability was described by a half-harmonic repulsive potential. This potential constitutes the "bottom" z-side of the boundary condition of the rectangular simulation box (see Fig. 1 *snapshot*).

Due to the charge of the headgroup layer, we also included a large excess of explicit electrolyte ions forming a background of 150 mM monovalent salt. In the ABSINTH model, the primary effect of the surrounding implicit solvent is in the DMFI, and, as long as the proteins do not penetrate the container walls, interactions in the interfacial layer should be approximated reasonably well by the simplified model we have chosen here. This is because the implicit hydrophobic solvation environment is never probed directly.

PrP^C is anchored to the membrane by a GPI moiety which is not represented explicitly in our simulations. To restrict the motion of PrP^C, we restrained, using quadratic flat-bottom potentials, the carbon atom of the C-terminal carboxyl group of residue S231 to within distances of 0.8–1.5 nm from the surface of the membrane mimic (46) (z-direction), and to an approximately central position in the x/y-directions. The latter was done to minimize the impact of the side walls of the simulation container, which are artificial.

Production simulations

All simulations were carried out using CAMPARI versions 3 or 4 (http://campari.sourceforge.net). The container was an aperiodic cubic box of 25 nm side length with soft walls represented by an atom-based half-harmonic potential for all six faces. As mentioned above, the "bottom" z-plane was treated as a mimic of a headgroup layer with excess negative charge. Explicit K^+ and Cl^- ions were added to neutralize the charges and create a salt concentration of 150 mM, which due to the large size of the box amounted to approximately 1400 excess ions per type. This is important to prevent an artificially high influence from the net charge of the headgroup layer.

The systems were propagated by means of a hybrid Monte Carlo (MC)/molecular dynamics (MD) sampler in the NVT ensemble. Stretches of 320 ps of MD were alternated with stretches composed of 16,000 elementary MC steps similar to prior work (47). The MC move set included pivot moves (48) on side-chain dihedrals (40%) and on backbone φ/ ψ angles (56%). The primary role of the MC segments was to allow rapid large-scale conformational changes of the flexible tail. In the MD stretches, the use of a dedicated integrator (49) allowed two important advantages: the use of a larger step (here, 5 fs) and explicit control over which internal degrees of freedom to sample. Here, we decided to constrain backbone dihedral angles for all ordered parts in both PrP^C and the antibodies. This is important because we employed the temperature replica-exchange method (50) to enhance sampling over an evenly spaced range of 24 temperatures from 305 K to 420 K for the unliganded systems and from 345 K to 460 K for the complexed systems. At high temperatures, the constraints ensure that there are no unwanted, partial unfolding events in the structured parts. Similarly, these constraints in conjunction with the interface modifications described above were sufficient to ensure that no unbinding of POM1 and POM6 occurred at any temperature. As indicated above, the translation of acetate molecules in the z-direction was constrained as well. Within each copy, temperature was maintained by an adapted Andersen thermostat (49,51) with a coupling time of 2 ps.

Swaps between neighboring replicas were attempted randomly every 8000 steps, i.e., 8 and 2 random swaps for each 64,000-step stretch of MD and each 16,000-step stretch of MC, respectively. Prior to the production simulations, each system was pre-equilibrated following the same protocol for 30 million steps. The production simulations ran for 50 million steps per replica, which corresponds to 0.2 μs of MD and 10 million MC steps per replica. Each system required approximately 2450 node hours, adding up to almost 22,000 node hours in total. The simulation system (i.e., number of nonbonding interactions) scaled up to six nodes, and thus each run required 17 days of wall clock time. The simulations were performed on the PizDaint (2 $\times$ 18 core CPUs Intel Xeon E5-2695 v4) and Eiger (2 $\times$ 64 core AMD EPYC 7742) supercomputers at the Swiss National Supercomputing Center in Lugano for the unliganded and the liganded systems, respectively. Nonbonded interactions were truncated with a residue-based cutoff of 1.2 nm with the exception of all charge-charge terms, which included all mobile ions (headgroups and salt) as well as all charged residues in proteins. This means that for large distances, a simplified monopole-monopole interaction was calculated for every pair. Trajectory data were saved every 4000 steps. Input files required for replicating the simulation settings exactly are available from the authors upon request.

The results and discussion section focuses on the sampling at 370 K. Results at other temperatures are provided in the supporting material. Note that there is not necessarily a stringent match between simulation and experimental temperatures because of the approximations inherent in the model (e.g., use of temperature-independent parameters, presence of constraints). Importantly, artifacts due to limited sampling are less likely to occur at elevated temperature.

RESULTS AND DISCUSSION

We first analyze the interactions between PrP^C and the membrane surface, followed by the contacts between the flexible tail and the globular domain. Both types of analysis are carried out for unliganded PrP^C (wild-type and six interstitial truncations of the flexible tail, see Fig. 1) and for the complexes of wild-type PrP^C with POM1 and POM6.

Interactions with the membrane surface

Cells that do not express PrP^C are not damaged by prion infection (52), which suggests that neurotoxicity arises from docking of PrP^{Sc} to PrP^C anchored at the membrane. Furthermore, ion channel-based toxicity triggered by a putative monomer has been characterized in association with various interstitial truncations in the flexible tail (20). Thus, we analyze here the effects of six such truncations, along with the influence of the Fab fragments of POM1 and the negative control POM6, on the distance of PrP^C from the membrane surface and their relative orientation. Notably, in our simulations, the complexes and protein folds are stable by design, and only the flexible tail can undergo large-scale conformational fluctuations while the entire assembly swivels around the anchor.

In all truncated systems and the wild-type, the average distance to the membrane surface is clearly more variable for the flexible tail than the globular domain of PrP^C (gray

area in Figs. 2, S1, and S2). Below, when we comment on distances, we also refer to their averages across the length of the simulation. An average distance of 2 nm by no means implies that the instantaneous distances never explore values close to zero, a fact illustrated by Videos S1, S2, and S3. The strongest differential signals in the distance between the flexible tail and the membrane surface are recorded by the binding of the antibodies along with the MutΔ105–125 truncation. The negatively charged cluster (CC1) of the MutΔ105–125 truncation is repelled by the membrane, which appears to push the entire tail away from the membrane surface toward distances in excess of 3 nm. Interestingly, the presence of the antibodies reduces by about 1–2 nm the average separation of the flexible tail from the membrane surface. The separation is about 3 nm in the unliganded wild-type PrP^C, and 1–2 nm in the complexed systems. In the latter, the two charged clusters are closer to the membrane ($\Delta \approx$ 1 nm separation) than in any unliganded system.

Concerning the globular domain, the interstitial truncations have marginal effects on its residue-wise proximity to the membrane. Fine details are only captured by analyzing the differential distance from wild-type (Fig. S2), which identifies a discriminatory signal for MutΔ105–125. The presence of the Fab fragments of POM1 and POM6 clearly reduces the distance of the globular domain to the membrane. The distance reduction is and must be due to a change in relative orientation with respect to the membrane's surface as the fold of the globular domain is preserved.

Because of the use of the replica-exchange protocol (see materials and methods), the data between nearby replicas are closely coupled. This is evident from Fig. S1, which reveals very systematic shifts with changes in temperature. The analysis here focuses on 370 K, an intermediate value. Note that thanks to the constraints and other approximations in the simulation model, the elevated temperatures are mainly a stratagem to improve sampling (see materials and methods). Importantly, there are two limits where different conclusions would be obtained: at the highest temperature shared by all runs, the tail is coil-like and universally distant from the membrane with the exception of the visible charge repulsion for the MutΔ105–125 variant; conversely, at the lowest shared temperatures, the behavior is increasingly heterogeneous and erratic and the distances to the membrane generally decrease. This regime offers too low sampling quality to arrive at meaningful conclusions, and the chosen value of 370 K is a compromise between maintaining the expected polymeric behavior of the tail and being able to sample the system with the resources at hand.

The distribution of the angles formed by the three α-helices and the membrane surface illustrate the orientational preference of the globular domain (Fig. 3). For the unliganded systems, all helices cover broad distributions of the angles, indicating a largely unrestricted tilting or swiveling motion of the globular domain. Except for the MutΔ105–125 truncation, the unliganded systems show essentially identical orientational disorder. Instead, the much narrower angular distributions in the presence of the Fab fragments of POM1 and POM6 indicate a substantially reduced orientational disorder (we calculated the information entropy of the distributions across 10 blocks for POM1, POM6, and wild-type: the resultant p-values of pairwise Wilcoxon tests are all less than 0.01). In these complexed systems, the domain preferentially samples a subspace of orientations, here manifest as a subset of tilt angles, which are less preferred in the unliganded systems. This is particularly visible for helices α_1 and α_2. Importantly, the overlap between preferred orientations in the presence or absence of antibody fragments is comparatively low, and this is evident for all three sets of distributions (see Fig. S3). The antibodies force the globular domain into a more tilted conformation that has it stacked onto the membrane surface, which is consistent with the reduced distances in Fig. 2. Notably, POM1 and POM6 have similar but not identical effects.

The effect of the antibodies on the orientation of the globular domain is also evident from the illustrative snapshots contained in Fig. 4 and from Videos S1, S2, and S3. This difference is less pronounced for α_3 whose C-terminal end is anchored to the membrane, and thus its flexibility is reduced in all systems. Fig. 2 reveals that there is no persistent association of flexible tail and membrane, and it can thus be expected that the truncations in the flexible tail have no substantial influence on the orientation of the globular domain (except for MutΔ105–125). Conversely, the reduction of orientational disorder in the presence of antibodies requires a more nuanced view. For example, the fragments of POM1 and POM6 carry opposite net charges (−6 and +9, respectively), so unlike for the MutΔ105–125 truncation, there is no simple net charge effect to invoke. What they share is a large exclusion volume that restricts the conformational freedom of both the globular domain and the flexible tail. Two signatures of this loss of freedom are a shift of the ensemble toward tail conformations where CC2 acts as something like a second anchor, and the globular domain being restricted to a more sideways orientation on the membrane.

Interactions between flexible tail and globular domain

In the wild-type PrP^C, all of the 100 residues of the flexible tail interact with a limited set of residues on the surface of the globular domain, as illustrated by the contact map (top left in Fig. 5).

Yet the region of the globular domain that is in contact with the flexible tail is only a minor part of its solvent-accessible surface. The main interaction region consists of the

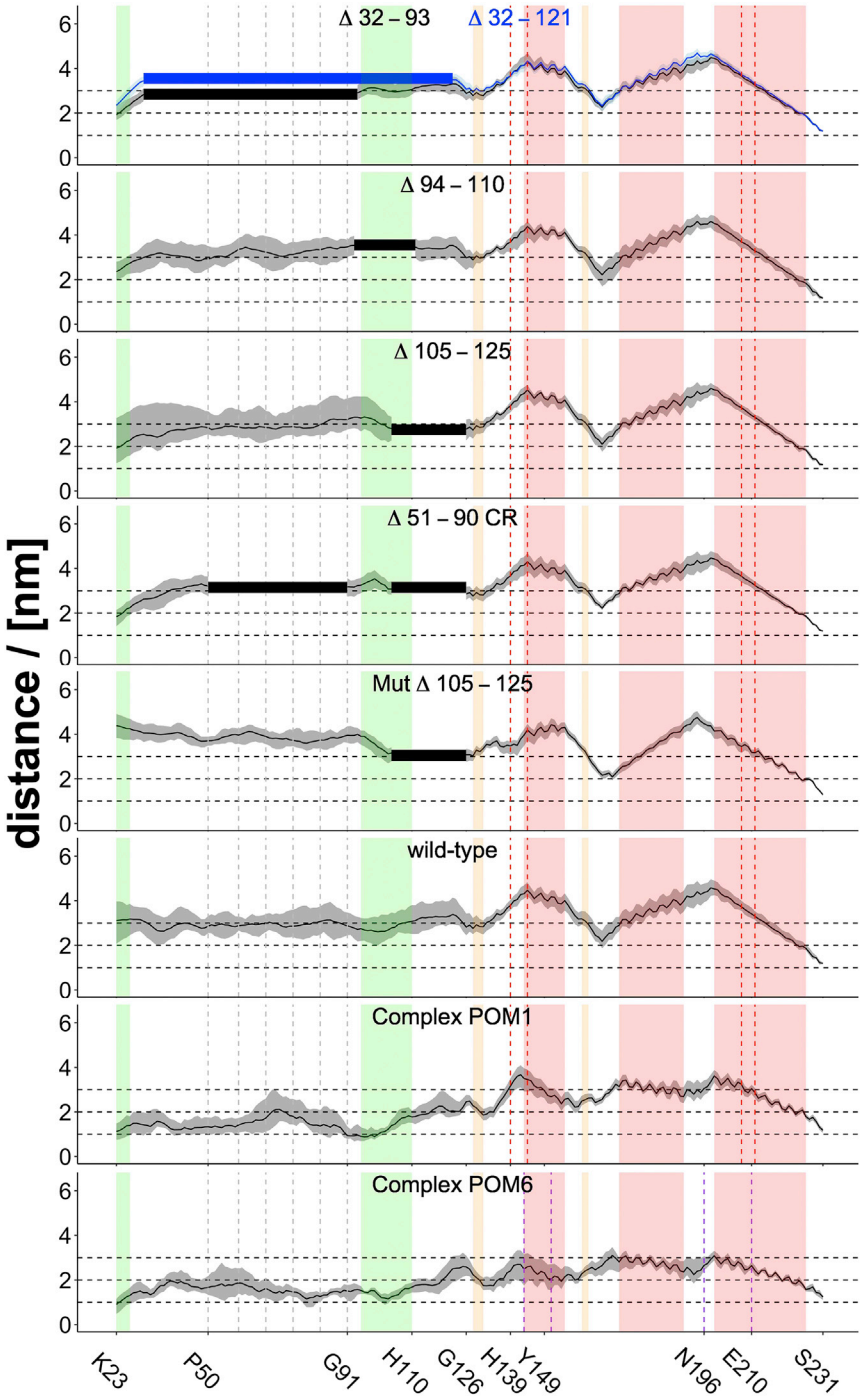

FIGURE 2 Average distance of PrP^C to the membrane surface. The C_α atoms were used to calculate the distance to the (x,y)-plane, which is the surface to which the centers of mass of the head group mimics are constrained (*solid line*, mean value; *gray area*, min/max errors from 10 equal blocks across the production portions of the simulations). The rectangles highlight the PrP^C α-helices (*red vertical rectangles*), β-strands (*orange*), charged clusters (*green*), and truncated segments (*black and blue horizontal rectangles*). The two regions of PrP^C that are in contact with the antibodies in the crystal structures ([6]),7 are highlighted (*red and purple dashed lines*). The horizontal dashed lines at 1 nm, 2 nm, and 3 nm are drawn to facilitate the comparison. To see this figure in color, go online.

two β-strands and the C-terminal segment of α_2 and is conserved irrespective of the variant under study (ribbon models in the top and bottom parts of Fig. 5). This is an interesting observation in itself, since it suggests that the free energy penalty for wrapping around and contacting other parts of the domain is too large to overcome given the largely compact/collapsed nature of the tail under these conditions (see Fig. 4). Irrespective of the truncation, there are no persistent interactions between the flexible tail and the two segments of the epitope. Only in the presence of POM6 one observes occasional interactions between the N-terminus of the flexible tail and the side chains of the D143-E151 segment.

The fact that the simulations with the truncated versions of the flexible tail preserve the same interaction sites on the globular domain as wild-type is actually surprising. This is true especially because the surface has no clear patterning of, for example, charged residues, with the

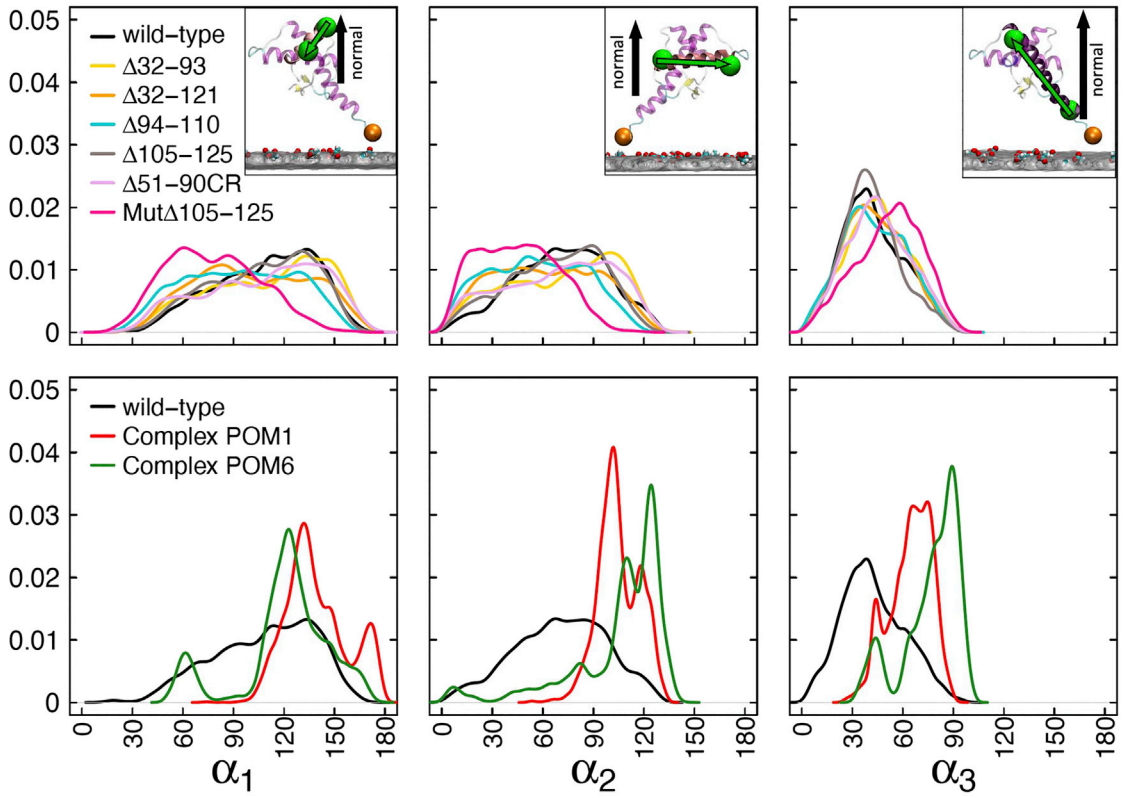

FIGURE 3 Orientation of the globular domain with respect to the membrane surface. Distributions of the angles between the helical axes and the normal to the membrane surface are shown. The helical axes are defined by the vectors between the centers of mass of the backbone atoms of residues D143 and R150, N172 and T189, and Y224 and T200, for helices α_1, α_2, and α_3, respectively. The latter vector is defined from the C-terminal to the N-terminal end of helix α_3 so that the angle is smaller than 90°. The snapshots in the upper right corners show the definition of the vectors, with the green arrows highlighting the helix vectors and the black arrow the normal to the membrane. The statistical significance of these distributions is assessed in Fig. S3. To see this figure in color, go online.

exception of the short helix α_1. Clearly, the residues involved in the tail cannot always be the same, leading to some diversity in interactions between the two main entities of PrP^C. For example, the flexible tails of the variants devoid of the octarepeat region (Δ32–93 and Δ51–90CR) record more abundant contacts with the β-sheet of the globular domain. As a second example, the MutΔ105–125 variant, which presents the strongest differential signal in Fig. 2,

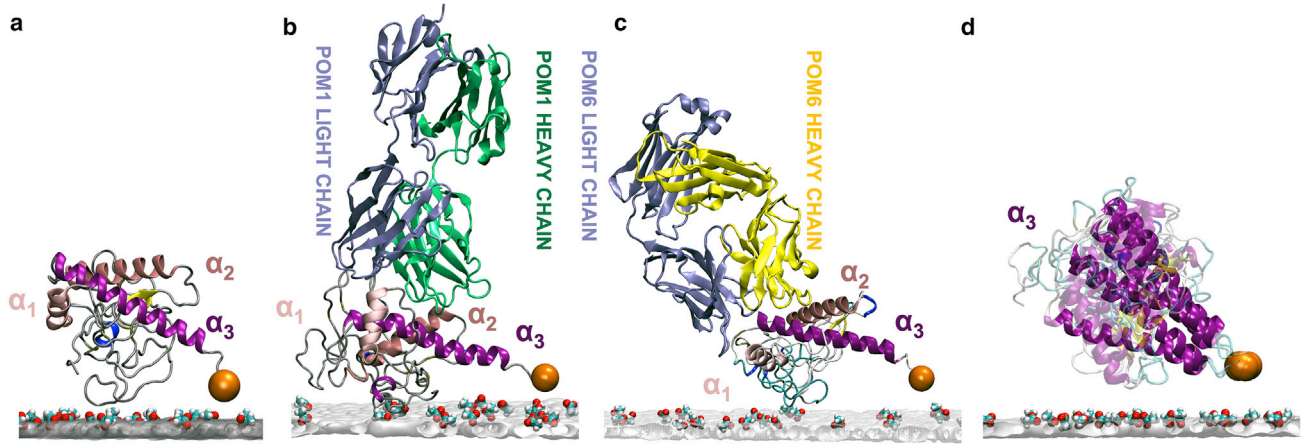

FIGURE 4 Simulation systems and orientational disorder. Representative snapshots of unliganded PrP^C (*a*), the PrP^C/POM1 complex (*b*), and the PrP^C/POM6 complex (*c*) are shown together with the membrane surface (*gray* with acetate ions colored by atomic element). The three α-helices and the β-sheet of PrP^C are highlighted (*purple and yellow ribbons*, respectively). (*d*) Four representative snapshots from the simulations of unliganded PrP^C are overlapped to visualize its flexibility. To see this figure in color, go online.

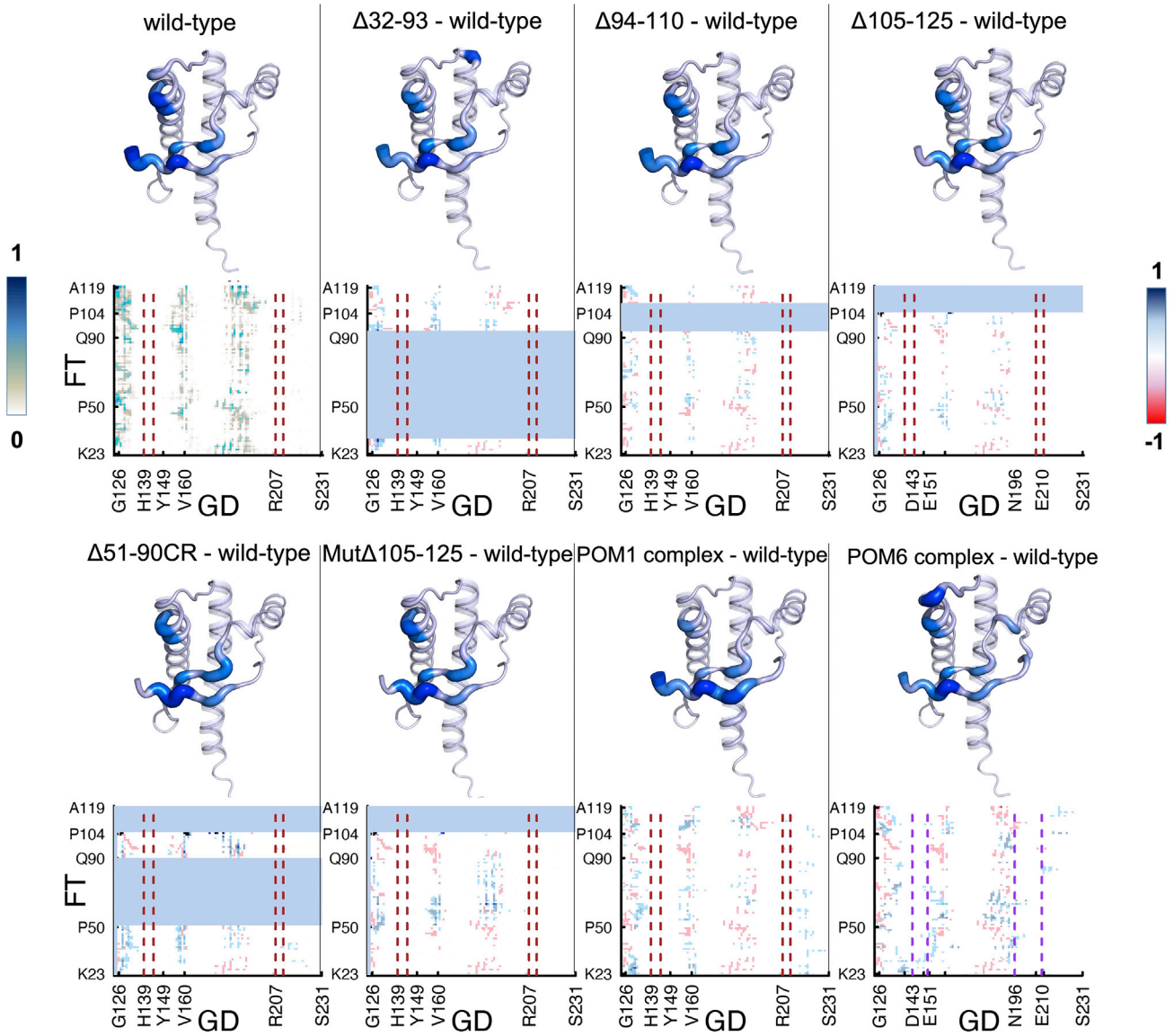

FIGURE 5 Contacts between the flexible tail and the globular domain. (*Center*) The matrix of pairwise contacts for the wild-type PrP^C (top, left, color bar on the left) shows the absolute frequencies while the other panels show differences relative to wild-type (higher or lower in *blue* and *red*, respectively, color bar on the right). The two regions of PrP^C that are in contact with the antibodies in the crystal structure are highlighted (*vertical dashed lines*). (*Top and bottom*) The ribbon models of the reference structure of the globular domain illustrate the frequency of contacts with the flexible tail (higher frequencies in darker colors and thicker ribbons). Two residues are considered to be in contact if the distance between any of their atoms is less than 0.5 nm. To probe the statistical significance of the data, Fig. S7 shows the average number of contacts between the flexible tail and the globular domain per globular domain residue. To see this figure in color, go online.

shows enhanced interactions of the segment 50–60 of the octapeptide region with the β-sheet and of residues 61–90 with α_2, and weaker contacts for the rest of the flexible tail. This trend of small incongruities between contact patterns continues for the liganded systems. POM1 binding leads to more frequent contacts between the N-terminus of the flexible tail and the β-sheet, reduced contacts with α_2, and more persistent interactions with α_3. Instead, POM6 docking extends the interaction hotspots on the surface of the globular domain to encompass the formation of more frequent contacts of the 50–70 segment with the C-terminus of α_2 and the C-terminus of α_1. Additionally, the C-terminus of the flexible tail forms more contacts with α_3.

The data in Fig. 5 suggest that the Δ94–110 truncation has the weakest impact relative to wild-type (light colors indicating small differences and a very similar structural visualization). At the other end of the spectrum, excluding dramatic truncations such as Δ51–90CR, the MutΔ105–125 variant as well as the POM6-bound form indicate the strongest shifts in contact patterns, which is intriguing since both are protective in admittedly different assays (10,20). To

quantify this ranking, Fig. S7 highlights the significance of differences in integrated contact probabilities on the globular domain relative to wild-type.

Overall, the simulation results presented above provide evidence that the interactions of the flexible tail, which is generally in a mostly collapsed conformation, with the globular domain are specific to each truncation and complexation (see Fig. 5). Even so, the binding of POM6 has clearly a larger effect on the interaction pattern than most of the sequence variants. These variants, unlike antibodies, have only a marginal effect on the relative orientation of the globular domain with respect to the membrane surface (see Figs. 3 and 4). The protective mutant MutΔ105–125 is the only variant or complex that increases the distance to the membrane surface of the flexible tail (Fig. 2). In contrast, the antibodies promote proximity of tail and membrane, with CC2 adopting a mediating function. None of these observations is tied to secondary structure formation in the tail (see Figs. S4–S6), which behaves like an intrinsically disordered protein of collapse-prone sequence composition (53).

DISCUSSION

Prion protein-induced neurotoxicity has been proposed to be modulated by the flexible tail of PrP^C (10,11). The tail's sequence composition puts it into the region normally occupied by folded proteins (53), and it has been shown to be essential for liquid-liquid phase separation (54) or to induce currents even when fused to an unrelated protein instead of the globular domain (23). Its primary role is thus very unlikely to be similar to that of an entropic brush but it rather appears to engage in multifarious interactions with itself, the globular domain, the membrane, and the antibodies. Various truncations in the flexible tail have been investigated to elucidate the details of the mechanisms of tail-mediated neurotoxicity and/or neuroprotection (12). Furthermore, monoclonal antibodies designed to recognize a variety of epitopes on the surface of PrP^C have proved to annihilate or induce toxicity (9). The monoclonal antibody POM1 binds to the globular domain of PrP^C and is neurotoxic, while POM6 recognizes a similar epitope as POM1 (though with a slightly larger contact surface (7)) and is innocuous (10). It has been proposed that POM1 toxicity, which has a phenotype similar to that of prion infection, originates from similarities in the docking of POM1 and PrP^{Sc} to PrP^C (10). It is necessary to keep in mind that the mechanism of antibody action on toxicity is complex. For example, earlier work highlighted that antioxidants block POM1 toxicity (55). More recently, it was shown that POM1 actually blocks amyloid formation for a specific mutant of the globular domain (56), that its neurotoxicity is rescued by a bispecific antibody targeting simultaneously an epitope in the flexible tail (57), or that current induction by POM1 was rescued by truncating residues 23–31 (23).

While a substantial amount of data has been acquired on cerebellar slices and mouse experiments (10), simulations can access high spatial resolution and thus provide insight at atomic level of detail on the effects of interstitial truncations of the flexible tail and POM1 and POM6 binding. The experimental evidence on the role of the flexible tail and the limited knowledge of its interactions with either membrane or antibodies motivated the present simulation study. In particular, we first analyzed the distance from and orientation relative to the membrane surface of full-length wild-type mouse PrP^C and six interstitial truncations of the flexible tail. Furthermore, we investigated the structural and dynamic effects of the binding of the Fab fragments of the two antibodies POM1 and POM6. To be able to obtain significant sampling for such large systems, we used hybrid rigid-body/torsional MC and MD simulations in implicit solvent with a stylized model of a negatively charged membrane surface. The main challenge was in sampling the flexible tail, and, to overcome it, we resorted to an advanced sampling technique (replica exchange) analyzed at elevated temperature while restraining the folded parts.

Three main observations emerge from the simulation results. First, different truncations in the flexible tail and the binding of antibodies influence the distance of PrP^C to the membrane. The strongest differential signals are recorded by the MutΔ105–125 truncation, which pushes the flexible tail away from the membrane, and the binding of the antibodies, which instead increase the average proximity of the flexible tail to the membrane by a similar shift. The flexible tail is devoid of regular elements of secondary structure, and its intrinsic disorder does not change upon antibody binding (see Figs. S4–S6), which seems to rule out the formation of β-sheets in the flexible tail as a toxicity mechanism. Experimental evidence suggests that the role of the flexible tail in toxicity is synergistic with the binding of PrP^{Sc} (or POM1) to the globular domain of PrP^C or with specific sequence truncations (10,12,23).

Second, the globular domain of PrP^C is located closer to the membrane in the presence of the antibodies than in the unliganded state. The distributions of the angles show that the orientational disorder of the globular domain is reduced in the presence of both antibody fragments, consistent with a tilting toward the membrane. Conversely, the different truncations have no effect on the orientation of the globular domain except for MutΔ105–125, which induces a shift in the weight in the distributions, generally in the opposite direction to the effect introduced by the antibodies.

Third, the contacts between flexible tail and globular domain involve all the residues of the former and only three segments of the latter, namely, the two-stranded β-sheet and the three C-terminal turns of α_2. Remarkably, while all contact patterns differ somewhat, it is the antibody fragments that have the strongest effects in terms of modulating which residues on the globular domain are involved (Figs. 5 and S7). This is despite the fact that they all use the full tail

(as in the wild-type), in contrast to the various truncations. It is worth noting that the interactions between flexible tail and the β-sheet in the globular domain are actually extended, and occasional contacts are formed with additional regions like α_3.

Caveats regarding statistical significance

The statistical significance of the data presented throughout this paper was probed by block averaging and by two-sample Wilcoxon tests (performed using built-in R functions (version 4.1.3) with default parameter choices). Generally, the data were split into 10 equal blocks across the ensemble. In Fig. 2, the min/max values across these block averages are shown directly to indicate variability. To identify the statistically relevant differences between systems, we compared the average quantities of any given system against the wild-type system. The statistically relevant points, i.e., those quantities that indicated a significant difference (p-value <0.05) from the wild-type system, are highlighted by the shaded area or by color-matching stars (Figs. S3 and S7). The stars were used in the plots only in case the standard error was too small for the shaded area to be visible.

There are several aspects to consider when quantifying uncertainty in this manner. First, we need to distinguish two sources of errors: those by choosing synchronized initial conditions (largely systematic) and those by random events occurring at equilibrium (statistical). The notion of independent repeats of entire simulations addresses the latter but only to an extent that is contingent upon the level of independence that can be achieved (58). Here, we studied a system that is split into initially randomized parts (ions, flexible tail) and more or less static parts (globular domain, antibodies). We also employed the replica-exchange method, which leads to ensemble averages constructed from discontinuous pieces of conformationally independent trajectories. From previous tests, we found that ensuring the randomness of starting structures, in particular the tail conformations, across all replicas for all systems is critical to avoid statistical errors from being masked by artificial initial state bias. This is a nontrivial but key concern when discussing the independence of, for example, repeat simulations. Initial state bias, which is exceptionally difficult to remove in post-processing (59), often leads to systematic relaxation effects as the system reaches equilibrium. This is not straightforwardly quantifiable in global terms, and we thus relied on the well-established heuristic of discarding long initial stretches as equilibration (i.e., 30 million steps) to minimize the impact of this relaxation period. From the remaining data, we compute the error and significance measures mentioned above. We had to rely on block averaging here because independent repeats of the simulations were out of reach in terms of computational resources. This is a caveat, as block averages still carry the additional danger of masking statistical errors through time correlation effects, which motivated the choice of comparatively few blocks. The situation is complicated further by the fact that replica exchange mixes different trajectories but does so in a stochastic manner. This means that the effective statistical "size" of a replica-exchange data set can vary strongly across conditions (here, temperatures), further obscuring statistical errors, and we have commented on the difficulty of dealing with such data sets in previous work (60,61). To quantify the level of mixing during the replica exchange, the average effective acceptance rate and number of unique geometric replicas visited are reported in Fig. S8. Readers should keep the discussion above in mind when evaluating the results.

Biological significance

The root of prion-induced toxicity remains elusive. Relying on experimental findings, several hypotheses were generated. On the one hand, prion pathogenesis is not linked to the loss of PrP^C function but rather to a gain of toxicity upon its conversion to PrP^{Sc} (10,62). On the other hand, prion-mediated toxicity was shown to be associated with misfolding and aggregation (63). Additionally, the toxicity induced by the interstitial truncations was proposed to originate from abnormal activity at the neuronal surface rather than from mislocalization or intracellular retention (62). Furthermore, *in vitro* and *in vivo* experimental data suggest that POM1 binding to membrane-anchored PrP^C mimics the toxic effect induced by PrP^{Sc} docking (10).

How do our computational results fit with existing experimental hypotheses? Before considering this question, it is important to point out that all proposed mechanisms of toxicity are well beyond the reach of atomistic simulations at this time. Our study provides a characterization of the conformational predisposition of the already complex system of a single, membrane-anchored, possibly liganded PrP^C toward the onset of such mechanisms. POM1 binding was proposed to emulate PrP^{Sc}-induced toxicity, thereby contributing to the misfolding of PrP^C (10,11). The POM1 and the POM6 Fab domains compete for the binding to the prion protein (7). The model introduced here reproduces the flexibility of the flexible tail, yet it cannot, by design, capture structural conversions in the globular domain (or the antibodies) due to the simulation setup (constraints imposed on the backbone dihedral angles of the ordered parts). Thereby, structural conversions in the globular domain remain a viable option to explain the opposite biological responses of POM1 and POM6.

Another proposed hypothesis links prion pathogenesis to the aggregation of multiple prion proteins on the membrane surface, which can induce membrane leakage (64). Here, we studied the effects of interstitial truncations and antibody binding on monomeric prion proteins. We show that the

flexible tail must be considered as being able to fulfill two somewhat antagonistic roles: sequestering parts of the globular domain surface from access by other species (shielding interaction sites) and promoting association with other species, including PrP^C, PrP^{Sc}, and antibodies (disordered but sticky). This is particularly important since the interactions between the flexible tail and the globular domain at the monomer level are comparatively sparse when considering the globular domain (Fig. 5). It is a straightforward conjecture that a second flexible tail will not be constrained to the same interaction hotspots on the globular domain. Clearly, studying the self-association of PrP^C (including the flexible tail) is a prerequisite to studying prion aggregation on the membrane surface. The complexity of investigating this using a similar, atomistic simulation protocol as described in this study will probably remain overwhelming in the immediate future.

Prion toxicity has also been correlated with the generation of spontaneous ionic currents (20,22, 23) and enhanced channel activity (65). Previous studies have shown that the interaction of the charges in the N-terminus of the flexible tail (CC1) with the membrane is essential for the generation of spontaneous ion currents, i.e., the deletion of or mutations in CC1 lead to no spontaneous ion currents (20,65). Furthermore, it has been recently demonstrated that POM1 binding enhances the channel activity of PrP^C(65). The simulations performed here are by design much more able to inform about the onset of an ion channel-based toxicity (triggered putatively by a monomer) than about an aggregation/conversion-based mechanism. Our results focus on the events prior to the generation of ionic currents and report on the possible interactions of the flexible tail with the membrane surface. If we accept this leap, our results show that current formation is not a simple function of proximity of the flexible tail to the membrane. For example, current-inducing truncations such as Δ105–125 do not differ in an obvious manner from the wild-type tail, which is innocuous. In fact, except for the MutΔ105–125 variant, the results in Figs. 2, 3, and 5 provide little evidence that the truncations exert their role through simple structure and shape considerations of the protein. Conversely, the strong differential effect recorded by the MutΔ105–125 truncation is a rather intuitive result of a charge inversion in one of the charged clusters. Furthermore, our results show that antibody binding decreases the overall distance of PrP^C to the membrane, independently of their biological response. Indeed, the binding of POM1 increases the proximity of PrP^C to the membrane, a conclusion supported by recent experimental findings (65), yet we find that POM6 has a similar effect.

CONCLUSION

In conclusion, we have assessed geometric parameters at atomic resolution that we hypothesized to be informative about the role of the flexible tail in the mechanism of prion disease. Surprisingly, we found stronger signals in these for the binding of antibody fragments than for experimentally established sequence truncations. The lack of a clear correlation between the experimentally known effect of a particular modification, which is often a complex, occasionally ambiguous manifestation in different types of experiments, is not necessarily surprising. Our data suggest the MutΔ105–125 variant is interpretable in simple electrostatic terms and that the two antibodies POM1 and POM6 do offer a differential signal, consistent with their contrasting effects. That said, the propensity to be toxic appears mostly related to mechanisms not captured by simulations (e.g., structural conversion in the globular domain, sequence specificities of membrane interactions).

Nevertheless, the present simulation results should spur the development of new agents (peptides, peptidomimetics, and organic compounds of low molecular weight) that bind to PrP^C to modulate its interactions with the membrane surface. A possible approach is to use simulation materials, methods, and protocols similar to those in this study to computationally design small molecules that interact with the flexible tail and/or promote its association with the globular domain of PrP^C. The experimental validation could make use of surface plasmon resonance to analyze the kinetics and thermodynamics of binding. The most promising candidates would then be evaluated in cellular assays, for example by quantification of their activity in rescuing prion-infected cultured organotypic cerebellar slices (66).

SUPPORTING MATERIAL

Supporting material can be found online at https://doi.org/10.1016/j.bpj.2022.06.007.

AUTHOR CONTRIBUTIONS

I.M.I., M.B., A.V., and A.C. designed the research. I.M.I. and M.B. carried out the simulations. All authors interpreted the data. I.M.I., A.V., and A.C. wrote the manuscript.

DECLARATION OF INTERESTS

The authors declare no competing interests.

ACKNOWLEDGMENTS

We thank Assunta Senatore and Adriano Aguzzi for suggesting the simulations of the POM1 complex and interesting discussions. The computational resources were provided by the Swiss National Supercomputing Center (CSCS) in Lugano. I.M.I. thanks the Peter und Traudl Engelhorn Foundation for a postdoctoral fellowship. This work was supported also by an Excellence grant of the Swiss National Science Foundation to A.C., the Synapsis Foundation-Alzheimer Research Switzerland, and the Heidi Seiler-Stiftung.

REFERENCES

1. Aguzzi, A., and A. M. Calella. 2009. Prions: protein aggregation and infectious diseases. *Physiol. Rev.* 89:1105–1152. https://doi.org/10.1152/physrev.00006.2009.
2. Stahl, N., D. R. Borchelt, …, S. B. Prusiner. 1987. Scrapie prion protein contains a phosphatidylinositol glycolipid. *Cell.* 51:229–240. https://doi.org/10.1016/0092-8674(87)90150-4.
3. Küffer, A., A. K. K. Lakkaraju, …, A. Aguzzi. 2016. The prion protein is an agonistic ligand of the G protein-coupled receptor Adgrg6. *Nature.* 536:464–468. https://doi.org/10.1038/nature19312.
4. Riesner, D. 2003. Biochemistry and structure of PrPC and PrPSc. *Br. Med. Bull.* 66:21–33. https://doi.org/10.1093/bmb/66.1.21.
5. Sigurdson, C. J., K. P. R. Nilsson, …, A. Aguzzi. 2009. De novo generation of a transmissible spongiform encephalopathy by mouse transgenesis. *Proc. Natl. Acad. Sci. USA.* 106:304–309. https://doi.org/10.1073/pnas.0810680105.
6. Baral, P. K., B. Wieland, …, M. N. G. James. 2012. Structural studies on the folded domain of the human prion protein bound to the Fab fragment of the antibody POM1. *Acta Crystallogr. D.* 68:1501–1512. https://doi.org/10.1107/s0907444912037328.
7. Baral, P. K., M. Swayampakula, …, M. N. G. James. 2018. Structural characterization of POM6 Fab and mouse prion protein complex identifies key regions for prions conformational conversion. *FEBS J.* 285:1701–1714. https://doi.org/10.1111/febs.14438.
8. White, A. R., P. Enever, …, S. Hawke. 2003. Monoclonal antibodies inhibit prion replication and delay the development of prion disease. *Nature.* 422:80–83. https://doi.org/10.1038/nature01457.
9. Polymenidou, M., R. Moos, …, A. Aguzzi. 2008. The POM monoclonals: a comprehensive set of antibodies to non-overlapping prion protein epitopes. *PLoS One.* 3:e3872. https://doi.org/10.1371/journal.pone.0003872.
10. Sonati, T., R. R. Reimann, A. Aguzzi…, 2013. The toxicity of antiprion antibodies is mediated by the flexible tail of the prion protein. *Nature.* 501:102–106. https://doi.org/10.1038/nature12402.
11. Dametto, P., A. K. K. Lakkaraju, …, A. Aguzzi. 2015. Neurodegeneration and unfolded-protein response in mice expressing a membrane-tethered flexible tail of PrP. *PLoS One.* 10:e0117412. https://doi.org/10.1371/journal.pone.0117412.
12. Beland, M., and X. Roucou. 2012. The prion protein unstructured N-terminal region is a broad-spectrum molecular sensor with diverse and contrasting potential functions. *J. Neurochem.* 120:853–868. https://doi.org/10.1111/j.1471-4159.2011.07613.x.
13. Rogers, M., F. Yehiely, …, S. B. Prusiner. 1993. Conversion of truncated and elongated prion proteins into the scrapie isoform in cultured cells. *Proc. Nat. Acad. Sci.USA.* 90:3182–3186. https://doi.org/10.1073/pnas.90.8.3182.
14. Flechsig, E., D. Shmerling, …, C. Weissmann. 2000. Prion protein devoid of the octapeptide repeat region restores susceptibility to scrapie in PrP knockout mice. *Neuron.* 27:399–408. https://doi.org/10.1016/s0896-6273(00)00046-5.
15. Shmerling, D., I. Hegyi, …, C. Weissmann. 1998. Expression of amino-terminally truncated PrP in the mouse leading to ataxia and specific cerebellar lesions. *Cell.* 93:203–214. https://doi.org/10.1016/s0092-8674(00)81572-x.
16. Li, A., H. M. Christensen, …, D. A. Harris. 2007. Neonatal lethality in transgenic mice expressing prion protein with a deletion of residues 105-125. *EMBO J.* 26:548–558. https://doi.org/10.1038/sj.emboj.7601507.
17. Bremer, J., F. Baumann, …, A. Aguzzi. 2010. Axonal prion protein is required for peripheral myelin maintenance. *Nat. Neurosci.* 13:310–318. https://doi.org/10.1038/nn.2483.
18. Baumann, F., M. Tolnay, …, A. Aguzzi. 2007. Lethal recessive myelin toxicity of prion protein lacking its central domain. *EMBO J.* 26:538–547. https://doi.org/10.1038/sj.emboj.7601510.
19. Brandner, S., and Z. Jaunmuktane. 2017. Prion disease: experimental models and reality. *Acta Neuropathol.* 133:197–222. https://doi.org/10.1007/s00401-017-1670-5.
20. Solomon, I. H., N. Khatri, …, D. A. Harris. 2011. An N-terminal polybasic domain and cell surface localization are required for mutant prion protein toxicity. *J. Biol. Chem.* 286:14724–14736. https://doi.org/10.1074/jbc.m110.214973.
21. Biasini, E., J. A. Turnbaugh, …, D. A. Harris. 2012. Prion protein at the crossroads of physiology and disease. *Trends Neur. Sci.* 35:92–103. https://doi.org/10.1016/j.tins.2011.10.002.
22. Solomon, I. H., E. Biasini, and D. A. Harris. 2012. Ion channels induced by the prion protein. *Prion.* 6:40–45. https://doi.org/10.4161/pri.6.1.18627.
23. Wu, B., A. J. McDonald, …, D. A. Harris. 2017. The N-terminus of the prion protein is a toxic effector regulated by the C-terminus. *Elife.* 6:e23473. https://doi.org/10.7554/elife.23473.
24. Morriss-Andrews, A., and J.-E. Shea. 2015. Computational studies of protein aggregation: methods and applications. *Annu. Rev. Phys. Chem.* 66:643–666. https://doi.org/10.1146/annurev-physchem-040513-103738.
25. Ilie, I. M., and A. Caflisch. 2019. Simulation studies of amyloidogenic polypeptides and their aggregates. *Chem. Rev.* 119:6956–6993. https://doi.org/10.1021/acs.chemrev.8b00731.
26. Caflisch, A. 2020. Kinetic control of amyloidogenesis calls for unconventional drugs to fight Alzheimer's disease. *ACS Chem. Neurosci.* 11:103–104. https://doi.org/10.1021/acschemneuro.9b00676.
27. Huang, D., and A. Caflisch. 2015. Evolutionary conserved Tyr169 stabilizes the $\beta2$–$\alpha2$ loop of the prion protein. *J. Am. Chem. Soc.* 137:2948–2957. https://doi.org/10.1021/ja511568m.
28. Hwang, W., S. Zhang, …, M. Karplus. 2004. Kinetic control of dimer structure formation in amyloid fibrillogenesis. *Proc. Natl. Acad. Sci. USA.* 101:12916–12921. https://doi.org/10.1073/pnas.0402634101.
29. Reddy, G., J. E. Straub, and D. Thirumalai. 2009. Dynamics of locking of peptides onto growing amyloid fibrils. *Proc. Natl. Acad. Sci. USA.* 106:11948–11953. https://doi.org/10.1073/pnas.0902473106.
30. Ilie, I. M., and A. Caflisch. 2018. Disorder at the tips of a disease-relevant Aβ42 amyloid fibril: a molecular dynamics study. *J. Phys. Chem. B.* 122:11072–11082. https://doi.org/10.1021/acs.jpcb.8b05236.
31. Bacci, M., J. Vymětal, …, A. Vitalis. 2017. Amyloid β fibril elongation by monomers involves disorder at the tip. *J. Chem. Theor. Comput.* 13:5117–5130. https://doi.org/10.1021/acs.jctc.7b00662.
32. Barducci, A., R. Chelli, …, M. Parrinello. 2006. Metadynamics simulation of prion protein: β-structure stability and the early stages of misfolding. *J. Am. Chem. Soc.* 128:2705–2710. https://doi.org/10.1021/ja057076l.
33. Chamachi, N. G., and S. Chakrabarty. 2017. Temperature-induced misfolding in prion protein: evidence of multiple partially disordered states stabilized by non-native hydrogen bonds. *Biochem.* 56:833–844. https://doi.org/10.1021/acs.biochem.6b01042.
34. van der Kamp, M. W., and V. Daggett. 2010. Influence of pH on the human prion protein: insights into the early steps of misfolding. *Biophys. J.* 99:2289–2298. https://doi.org/10.1016/j.bpj.2010.07.063.
35. Caldarulo, E., A. Barducci, …, M. Parrinello. 2017. Prion protein $\beta2$–$\alpha2$ loop conformational landscape. *Proc. Natl. Acad. Sci. USA.* 114:9617–9622. https://doi.org/10.1073/pnas.1712155114.
36. Zhou, S., D. Shi, …, H. Liu. 2019. pH-induced misfolding mechanism of prion protein: insights from microsecond-accelerated molecular dynamics simulations. *ACS Chem. Neurosci.* 10:2718–2729. https://doi.org/10.1021/acschemneuro.8b00582.
37. Frontzek, K., M. Bardelli, …, A. Aguzzi. 2021. A conformational switch controlling the toxicity of the prion protein. Preprint at bioRxiv. https://doi.org/10.1101/2021.09.20.460912.
38. Gossert, A. D., S. Bonjour, …, K. Wüthrich. 2005. Prion protein NMR structures of elk and of mouse/elk hybrids. *Proc. Natl. Acad. Sci. USA.* 102:646–650. https://doi.org/10.1073/pnas.0409008102.

39. Engh, R. A., and R. Huber. 1991. Accurate bond and angle parameters for X-ray protein structure refinement. *Acta Crystallogr. A.* 47:392–400. https://doi.org/10.1107/s0108767391001071.

40. Vitalis, A., and R. V. Pappu. 2009. ABSINTH: a new continuum solvation model for simulations of polypeptides in aqueous solutions. *J. Comput. Chem.* 30:673–699. https://doi.org/10.1002/jcc.21005.

41. Huang, J., and A. D. MacKerell. 2013. CHARMM36 all-atom additive protein force field: validation based on comparison to NMR data. *J. Comput. Chem.* 34:2135–2145. https://doi.org/10.1002/jcc.23354.

42. Marchand, J.-R., T. Knehans, …, A. Vitalis. 2020. An ABSINTH-based protocol for predicting binding affinities between proteins and small molecules. *J. Chem. Inf. Model.* 60:5188–5202. https://doi.org/10.1021/acs.jcim.0c00558.

43. Vitalis, A., and A. Caflisch. 2010. Micelle-like architecture of the monomer ensemble of Alzheimer's amyloid-β peptide in aqueous solution and its implications for aβ aggregation. *J. Mol. Biol.* 403:148–165. https://doi.org/10.1016/j.jmb.2010.08.003.

44. Arnon, Z., A. Vitalis, …, E. Gazit. 2016. Dynamic microfluidic control of supramolecular peptide self-assembly. *Nat. Commun.* 7:13190. https://doi.org/10.1038/ncomms13190.

45. Nagle, J. 1993. Area/lipid of bilayers from NMR. *Biophys. J.* 64:1476–1481. https://doi.org/10.1016/s0006-3495(93)81514-5.

46. Zuegg, J., and J. E. Gready. 2000. Molecular dynamics simulation of human prion protein including both N-linked oligosaccharides and the GPI anchor. *Glycobiology.* 10:959–974. https://doi.org/10.1093/glycob/10.10.959.

47. Vitalis, A., and A. Caflisch. 2014. Equilibrium sampling approach to the interpretation of electron density maps. *Structure.* 22:156–167. https://doi.org/10.1016/j.str.2013.10.014.

48. Vitalis, A., and R. V. Pappu. 2009. Methods for Monte Carlo simulations of biomacromolecules. *Annu. Rep. Comput. Chem.* 5:49–76. https://doi.org/10.1016/S1574-1400(09)00503-9.

49. Vitalis, A., and R. V. Pappu. 2014. A simple molecular mechanics integrator in mixed rigid body and dihedral angle space. *J. Chem. Phys.* 141:034105. https://doi.org/10.1063/1.4887339.

50. Swendsen, R. H., and J.-S. Wang. 1986. Replica Monte Carlo simulation of spin-glasses. *Phys. Rev. Lett.* 57:2607–2609. https://doi.org/10.1103/physrevlett.57.2607.

51. Andersen, H. C. 1980. Molecular dynamics simulations at constant pressure and/or temperature. *J. Chem. Phys.* 72:2384–2393. https://doi.org/10.1063/1.439486.

52. Brandner, S., S. Isenmann, …, A. Aguzzi. 1996. Normal host prion protein necessary for scrapie-induced neurotoxicity. *Nature.* 379:339–343. https://doi.org/10.1038/379339a0.

53. Das, R. K., and R. V. Pappu. 2013. Conformations of intrinsically disordered proteins are influenced by linear sequence distributions of oppositely charged residues. *Proc. Natl. Acad. Sci. USA.* 110:13392–13397. https://doi.org/10.1073/pnas.1304749110.

54. Tange, H., D. Ishibashi, …, N. Nishida. 2021. Liquid – liquid phase separation of full-length prion protein initiates conformational conversion in vitro. *J. Biol. Chem.* 296:100367. https://doi.org/10.1016/j.jbc.2021.100367.

55. Herrmann, U. S., T. Sonati, …, A. Aguzzi. 2015. Prion infections and anti-PrP antibodies trigger converging neurotoxic pathways. *PLoS Pathog.* 11:e1004662. https://doi.org/10.1371/journal.ppat.1004662.

56. Sanz-Hernández, M., J. D. Barritt, …, A. De Simone. 2021. Mechanism of misfolding of the human prion protein revealed by a pathological mutation. *Proc. Natl. Acad. Sci. USA.* 118. . e2019631118. https://doi.org/10.1073/pnas.2019631118.

57. Bardelli, M., K. Frontzek, L. Varani…, 2018. A bispecific immunotweezer prevents soluble PrP oligomers and abolishes prion toxicity. *PLoS Pathog.* 14:1–22. https://doi.org/10.1371/journal.ppat.1007335.

58. Grossfield, A., P. N. Patrone, …, D. M. Zuckerman. 2018. Best practices for quantification of uncertainty and sampling quality in molecular simulations (article v1.0). *Living J. Comput. Mol. Sci.* 1:5067. https://doi.org/10.33011/livecoms.1.1.5067.

59. Bacci, M., A. Caflisch, and A. Vitalis. 2019. On the removal of initial state bias from simulation data. *J. Chem. Phys.* 150:104105. https://doi.org/10.1063/1.5063556.

60. Bacci, M., A. Vitalis, and A. Caflisch. 2015. A molecular simulation protocol to avoid sampling redundancy and discover new states. *Biochim. Biophys. Acta Gen. Subj.* 1850:889–902. https://doi.org/10.1016/j.bbagen.2014.08.013.

61. Muff, S., and A. Caflisch. 2009. ETNA: equilibrium transitions network and arrhenius equation for extracting folding kinetics from REMD simulations. *J. Phys. Chem. B.* 113:3218–3226. https://doi.org/10.1021/jp807261h.

62. Chiesa, R. 2015. The elusive role of the prion protein and the mechanism of toxicity in prion disease. *PLoS Pathog.* 11:e1004745. https://doi.org/10.1371/journal.ppat.1004745.

63. Moreno, J. A., H. Radford, …, C. A. Ortori. 2012. Sustained translational repression by eIF2α–P mediates prion neurodegeneration. *Nature.* 485:507–511. https://doi.org/10.1038/nature11058.

64. Ambadi Thody, S., M. Mathew, and J. B. Udgaonkar. 2018. Mechanism of aggregation and membrane interactions of mammalian prion protein. *Biochim. Biophys. Acta Biomembr.* 1860:1927–1935. https://doi.org/10.1016/j.bbamem.2018.02.031.

65. Wu, J., A. Lakkaraju, A. Aguzzi, and J. Luo. 2022. The channel activities of the full-length prion and truncated proteins. Preprint at bioRxiv. https://doi.org/10.1101/2022.01.12.475988.

66. Falsig, J., T. Sonati, …, A. Aguzzi. 2012. Prion pathogenesis is faithfully reproduced in cerebellar organotypic slice cultures. *PLoS Pathog.* 8:e1002985. https://doi.org/10.1371/journal.ppat.1002985.

Biophysical Journal, Volume *121*

Supplemental information

Antibody binding modulates the dynamics of the membrane-bound prion protein

Ioana M. Ilie, Marco Bacci, Andreas Vitalis, and Amedeo Caflisch

Manuscript submitted to **Biophysical***Journal*
Article

Supplementary Material: Antibody binding modulates the dynamics of the membrane-bound prion protein

Ioana M. Ilie[1], Marco Bacci[1], Andreas Vitalis[1], and Amedeo Caflisch[1,*]

[1]Department of Biochemistry, University of Zürich, Zürich, Switzerland
[*]Correspondence: caflisch@bioc.uzh.ch

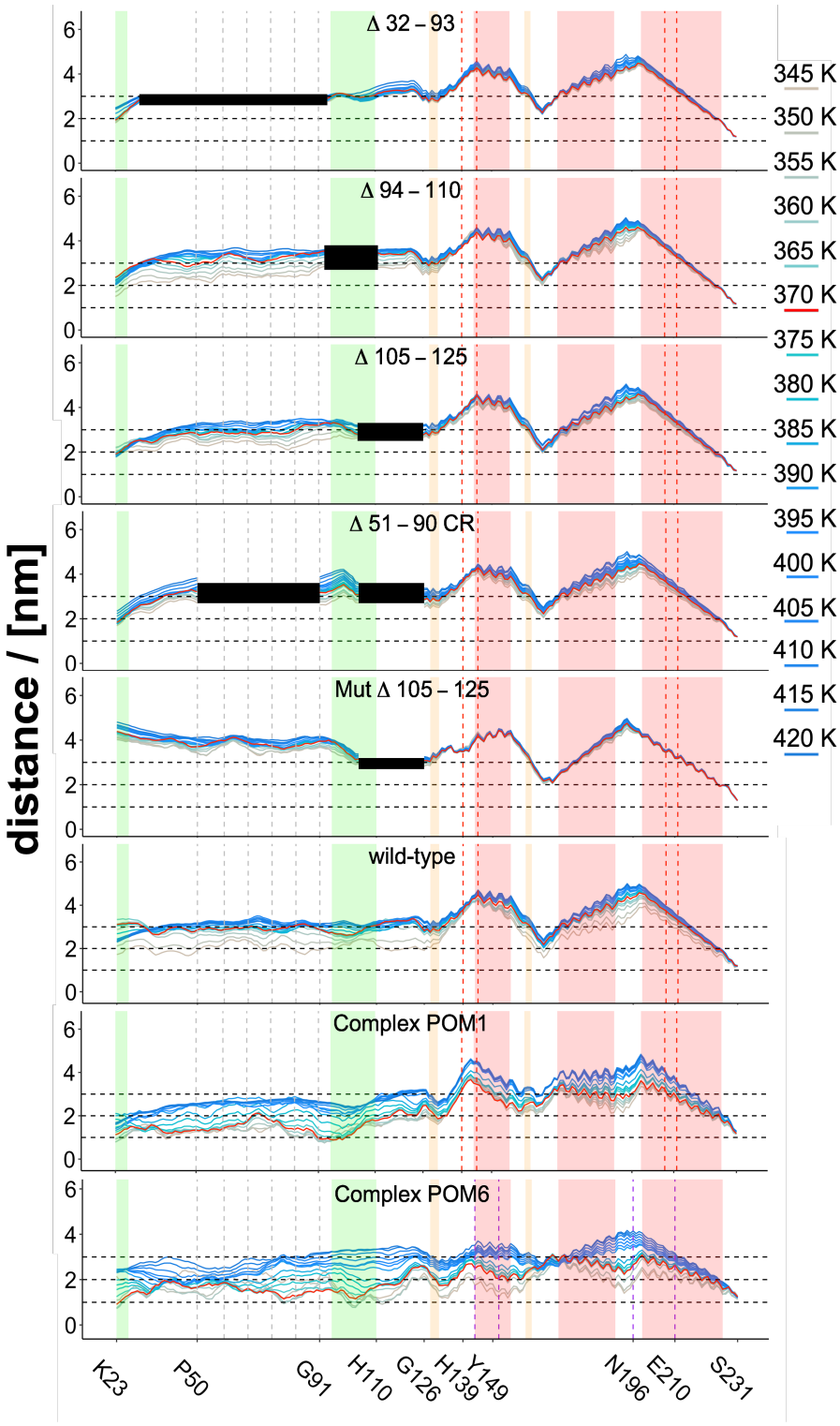

Figure S1: **Distance of PrP^C to the membrane surface for temperatures between 345 and 420 K.** The C_α atoms were used to calculate the distances to the (x,y)-plane as in Fig. 2 in the main text. At lower temperatures (light colours), shorter average distances to the membrane are sampled, and higher temperatures (darker colours) push PrP^C further away from the membrane surface. The rectangles highlight the PrP^C α-helices (red vertical rectangles), β-strands (orange), charged clusters (green), and truncated segments (black and blue horizontal rectangles). The two regions of PrP^C that are in contact with the antibodies in the crystal structure are highlighted (red and purple vertical dashed lines for POM1 and POM6, respectively). The horizontal dashed lines at 1.0 nm, 2.0 nm and 3.0 nm are drawn to facilitate comparisons across panels.

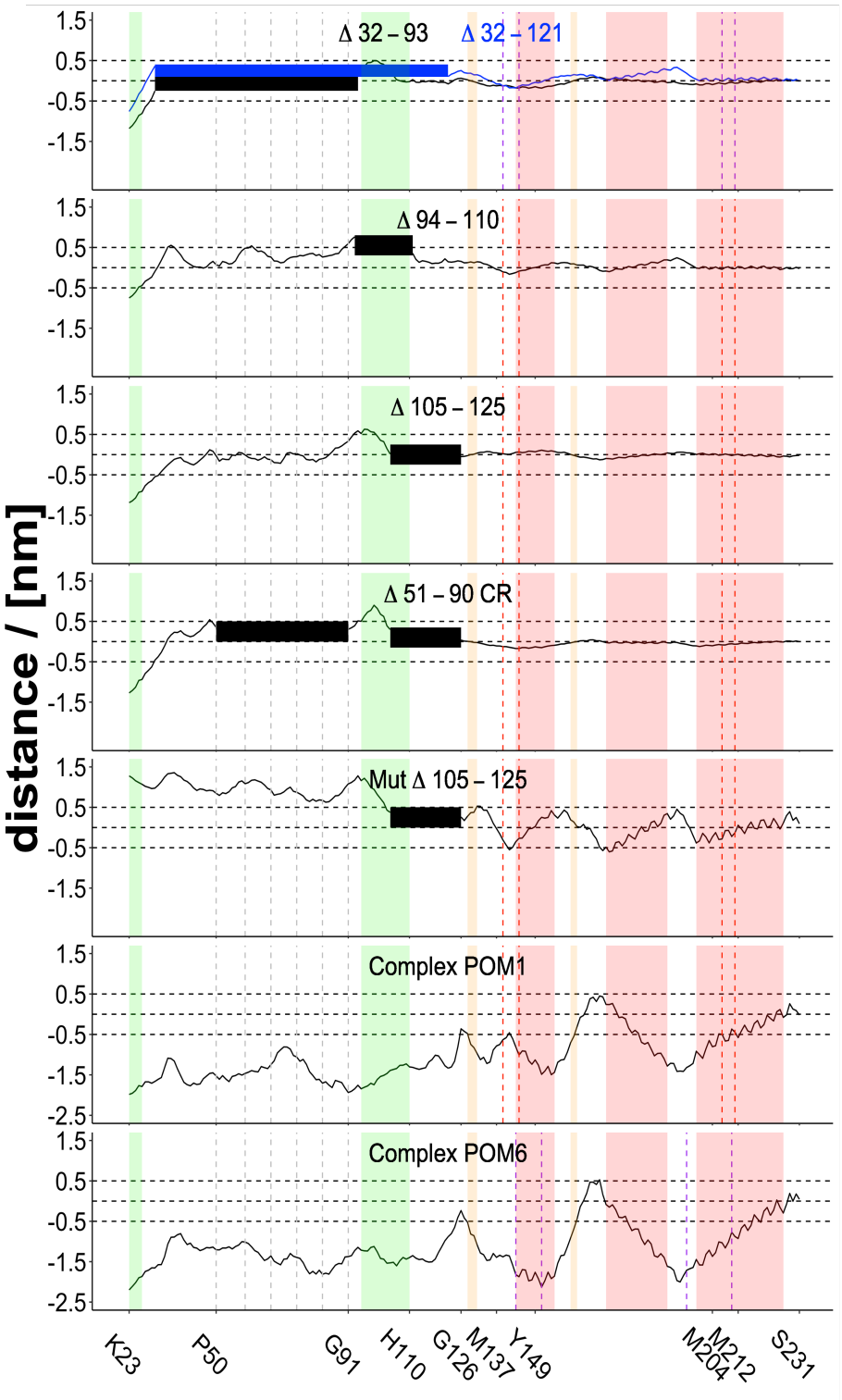

Figure S2: **Distance difference of PrP^C to the membrane between each variant and wild-type PrP^C at 370 K.** The C_α atoms were used to calculate the distances to the (x,y)-plane. The rectangles highlight the PrP^C α-helices (red vertical rectangles), β-strands (orange), charged clusters (green), and truncated segments (black and blue horizontal rectangles). The two regions of PrP^C that are in contact with the antibodies in the crystal structure are highlighted (red and purple vertical dashed lines for POM1 and POM6, respectively). The horizontal dashed lines at -0.5 nm, 0.0 nm and 0.5 nm are drawn to facilitate the comparison.

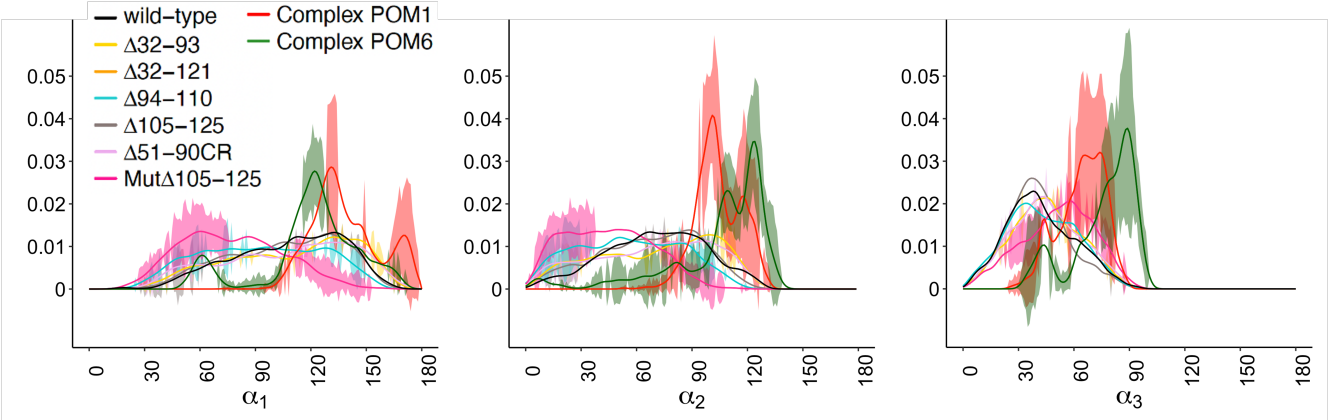

Figure S3: **Orientation of the globular domain with respect to the membrane surface.** The shaded area represents the standard error of the mean evaluated as the standard deviation of ten probability distributions along ten blocks equally spaced along the trajectory. These shaded errors are shown only whenever a two-sample Wilcoxon test (computed using standard R functions) comparing averages of any given system against the wild-type system indicated significant differences (p-value < 0.05).

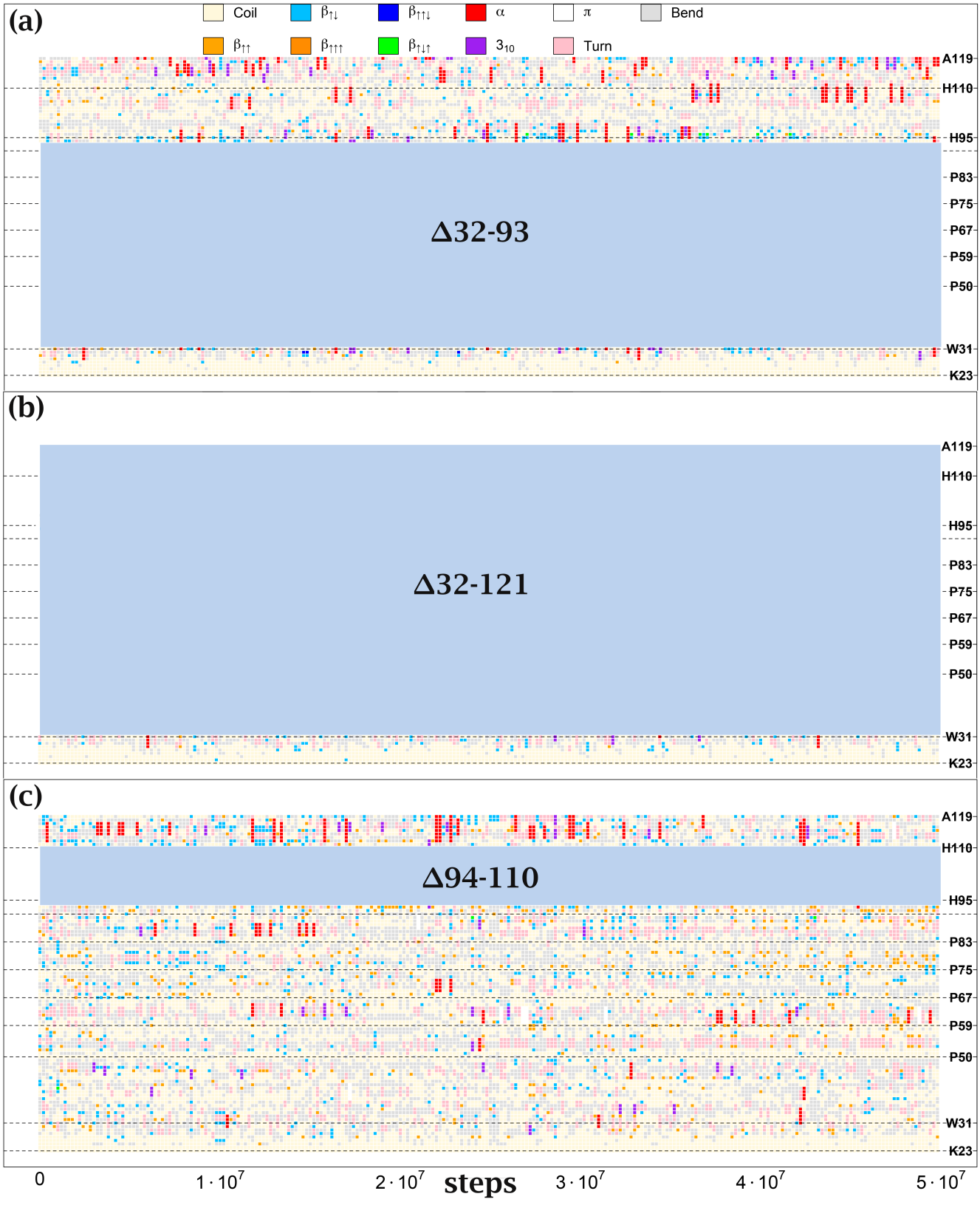

Figure S4: **Secondary structure assignment per residue in the flexible tail at T = 370 K.** The horizontal dashed lines delimit the key regions in the flexible tail, *i.e.* CC1, the octarepeats and CC2. The systems were propagated over 50 million steps in the canonical ensemble.

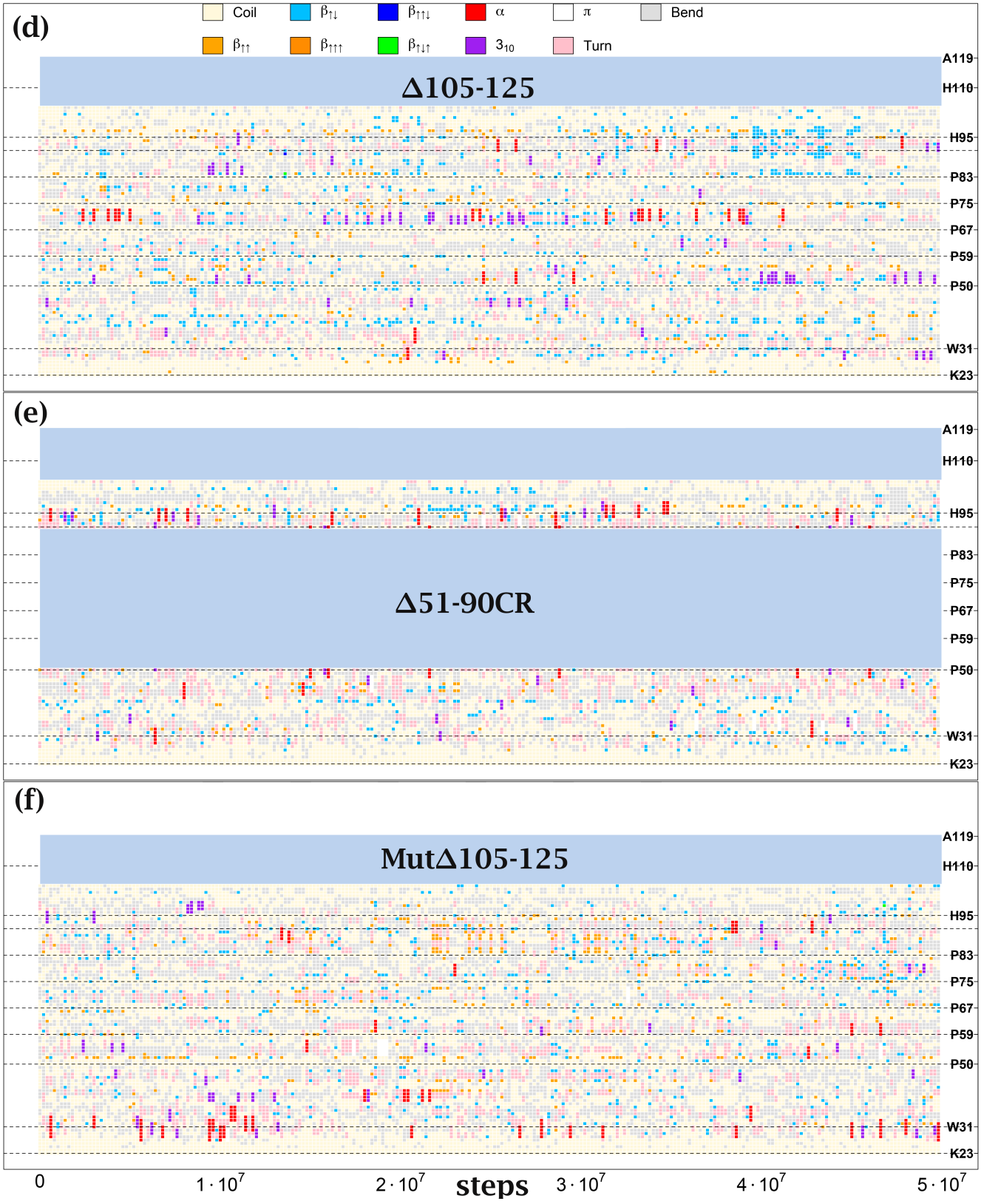

Figure S5: **Secondary structure assignment per residue in the flexible tail at T = 370 K.** See caption Fig. S4.

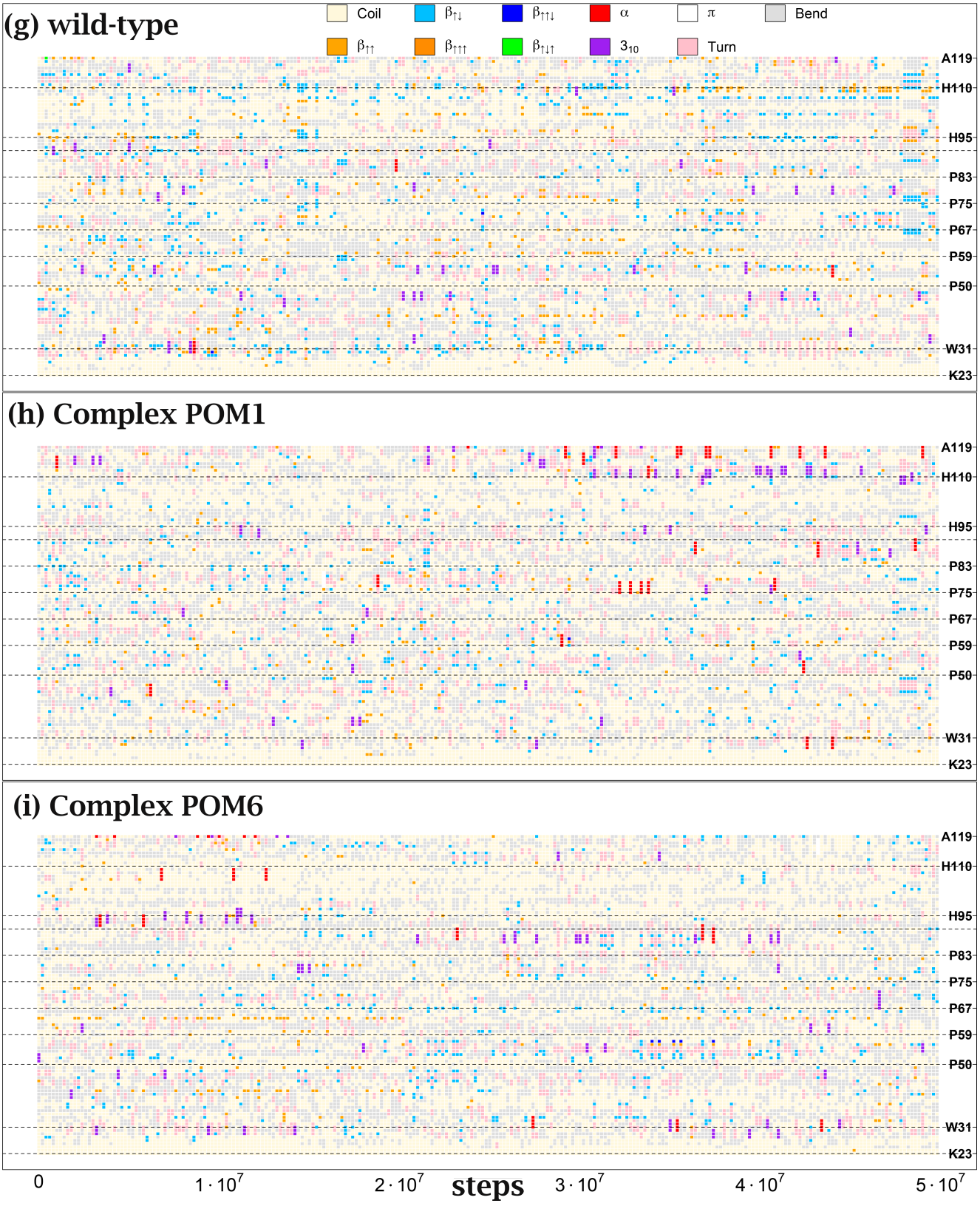

Figure S6: **Secondary structure assignment per residue in the flexible tail at T = 370 K.** See caption Fig. S4.

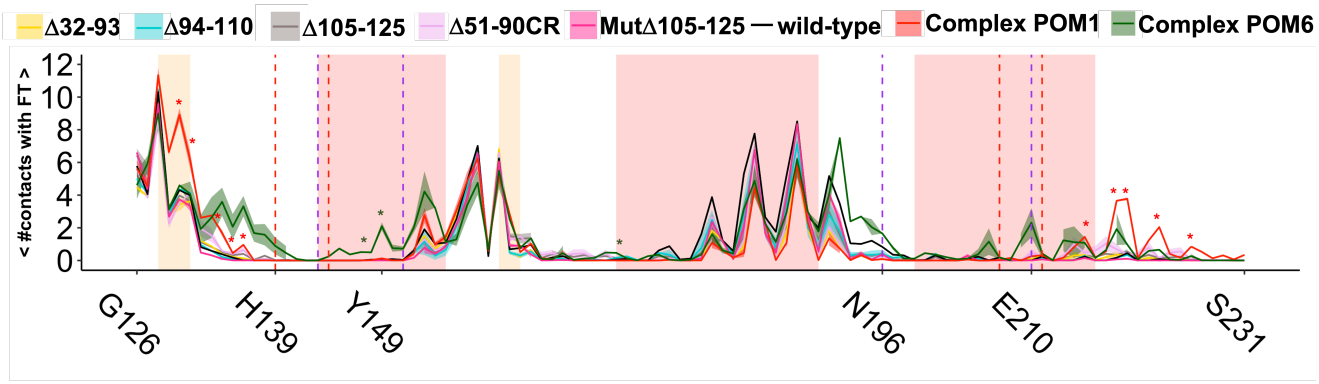

Figure S7: **Average number of contacts between the flexible tail and the globular domain.** This plot is essentially the result of integrating the contact maps in Fig. 5 across the flexible tail dimension. The shaded area represents the standard error of the mean evaluated as the standard deviation of ten average values along ten blocks equally spaced blocks along the trajectory. These shaded errors are shown only whenever a two-sample Wilcoxon test (computed using standard R functions) comparing averages of any given system against the wild-type system indicated significant differences (p-value < 0.05). In case the standard error was too small to be visualized, color matching stars were added instead. The rectangles highlight the PrP^C α-helices (red vertical rectangles), β-strands (orange) and charged clusters (green). The two regions of PrP^C that are in contact with the antibodies in the crystal structures (1) (2) are highlighted (red and purple dashed lines).

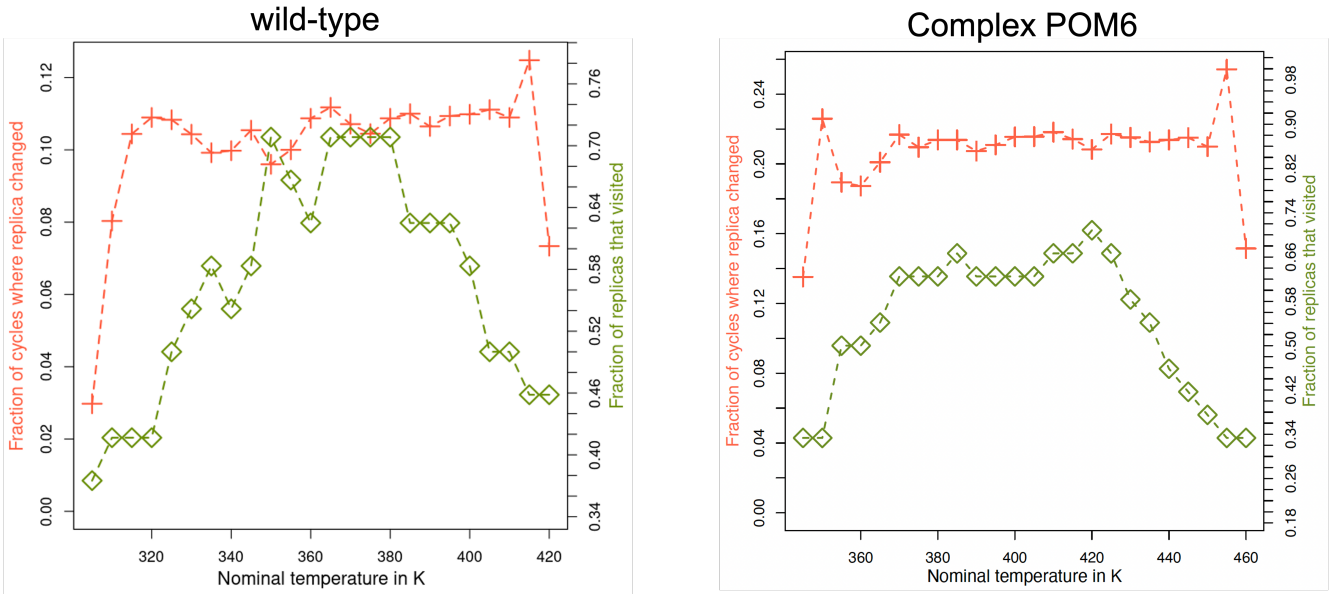

Figure S8: **Average effective acceptance rate and number of unique geometric replicas visited.** This plot shows the average effective acceptance rate as a function of nominal temperature (red line) along with the number of unique geometric replicas that visited that nominal temperature (green line) for wild-type and the POM6 complex. Both measures show drop-offs at both limits and less than 100 % visitation throughout.

Movie S1 Orientational disorder of unliganded PrP^C at an average temperature of 400 K. The movie of the unrexed trajectory shows the orientational flexibility of PrP^C with respect to the membrane surface.

Movie S2 Restricted orientational disorder of PrP^C in complex with POM1 at an average temperature of 400 K. The movie of the unrexed trajectory shows the closer distance to the membrane surface and restricted orientational disorder of PrP^C compared to the unliganded state.

Movie S3 Restricted orientational disorder of PrP^C in complex with POM6 at an average temperature of 400 K. The movie of the unrexed trajectory shows the closer distance of the GD to the membrane surface and restricted orientational disorder of PrP^C compared to the unliganded state.

REFERENCES

1. Baral, P., B. Wieland, M. Swayampakula, M. Polymenidou, M. Rahman, N. Kav, A. Aguzzi, and M. James, 2012. Structural studies on the folded domain of the human prion protein bound to the Fab fragment of the antibody POM1. *ACTA CRYSTALLOGR D* 68:1501–12.

2. Baral, P. K., M. Swayampakula, A. Aguzzi, and M. N. G. James, 2018. Structural characterization of POM6 Fab and mouse prion protein complex identifies key regions for prions conformational conversion. *FEBS J.* 285:1701–1714.